Electronic Supplementary Material (ESI) for Journal of Materials Chemistry A.

Supporting Information

Manipulation on crystallization of perovskite films induced by a rotating magnetic field during the blade coating in air

Yichuan Lin,[a] Xiaoqin Ye,[b] Zhiming Wu,[a] Chunquan Zhang,[a] Yulong Zhang,[a] Haifeng Su,[c]
Jun Yin,*[a] and Jing Li*[a]

[a]. A Collaborative Innovation Center for Optoelectronic Semiconductors and Efficient Devices, Department of Physics / Pen-Tung Sah Institute of Micro-Nano Science and Technology, Xiamen University, Xiamen, 361005, China

[b]. State Key Laboratory of Materials Processing and Die & Mold Technology, School of Materials Science and Engineering, Huazhong University of Science and Technology (HUST), Wuhan 430074, China.

[c]. College of Chemistry and Chemical Engineering, Xiamen University, Xiamen, 361005, China.

*E-mail: lijing@xmu.edu.cn or jyin@xmu.edu.cn.

S1. SEM images of RMF-induced perovskite thin-films

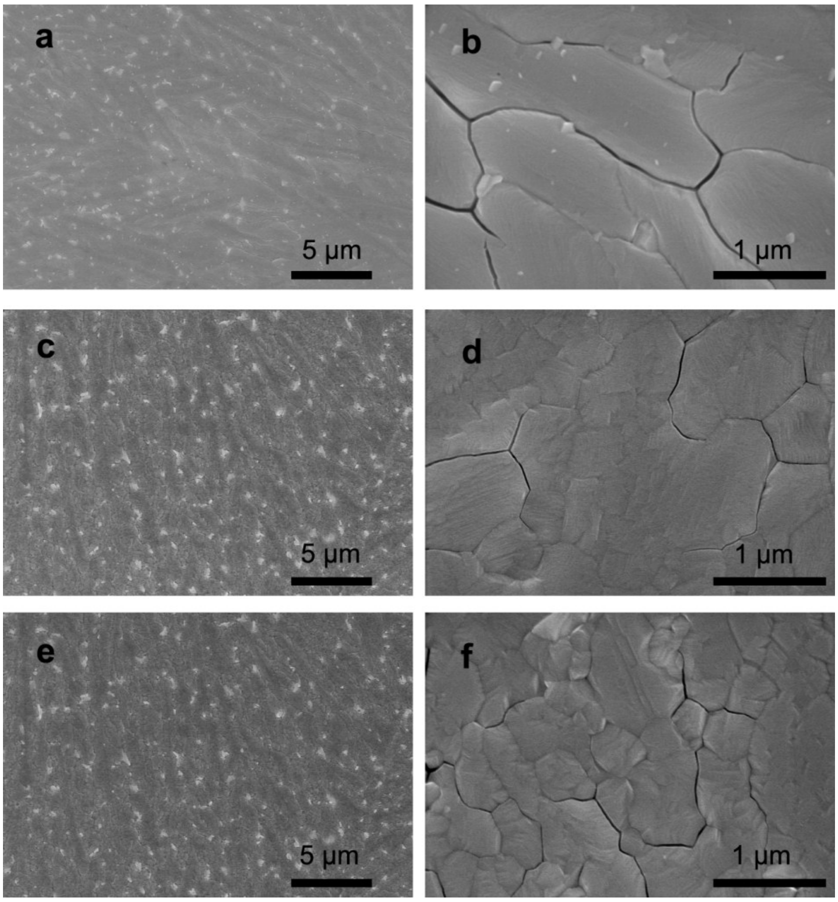

Fig. S1. SEM images of RMF-induced perovskite thin-films fabricated by varying the rotation rate at (a)-(b) 350 rpm, (c)-(d) 700 rpm, and (e)-(f) 1050 rpm in different magnifications. All cracks in (b), (d) and (f) were caused by electronic beam scanning.

S2. Analysis of the Lorentz force and the related electric/magnetic field during the blade-coating under RMF

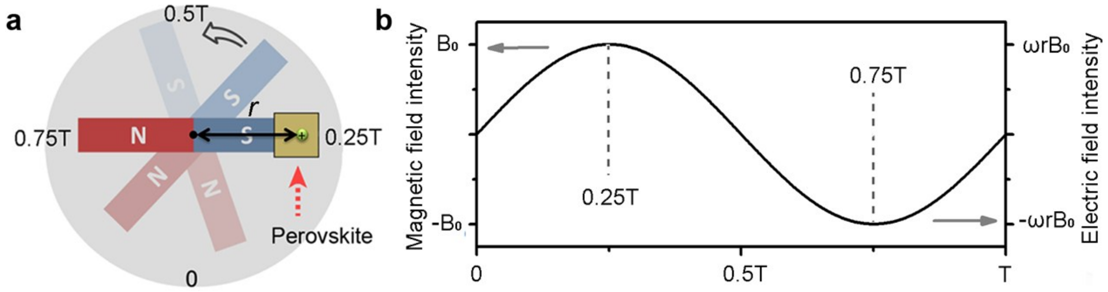

Fig. S2. (a) Schematic illustration of the coating region under RMF. (b) Variation curve of magnetic field intensity (MFI) and electric field intensity (EFI) near the perovskite film within a rotation period of *T*.

In the blade-coating process, as discussed in the main text, the charged particles in the precursor solution, such as the cationic MA^+, would experience the Lorentz force (*F*) under the sinusoidal magnetic field. And the Lorentz force (*F*) is given by:

$$\boldsymbol{F} = q\boldsymbol{v}\times\boldsymbol{B} \tag{1}$$

where q is elementary charge, $\boldsymbol{v}$ is the linear velocity of the charged particles on the substrate. Here, the value of $\boldsymbol{B}$ is a sinusoidal function and can be described as:

$$|\boldsymbol{B}| = B_0 sin(\omega t) \tag{2}$$

Here, B_0 is the initial invariable magnetic field intensity. ω is the angular frequency of the sinusoidal magnetic field, and can be calculated by $\omega=2\pi/T$ (T is the period of the sine function). And the value of $\boldsymbol{v}$ is given by:

$$|\boldsymbol{v}| = \omega r \tag{3}$$

where r is the radius of the rotating magnetic field, as illustrated in Fig. S2a.

As the Lorentz force (***F***) also can be considered as the equivalent electric field force, the value of ***F*** can be described as:

$$|\boldsymbol{F}| = q|\boldsymbol{v}||\boldsymbol{B}| = q|\boldsymbol{E}| \tag{3}$$

Therefore, the equivalent electric field magnitude ($|\boldsymbol{E}|$) can be expressed as $|\boldsymbol{E}| = |\boldsymbol{v}||\boldsymbol{B}| = \omega r|\boldsymbol{B}| = \omega r B_0 sin(\omega t)$, and the variation curve of electric field magnitude ($|\boldsymbol{E}|$) versus rotation angle has the same tend as that of magnetic field, as illustrated in Fig. S2b.

S3. Estimation of the nucleation threshold for the perovskite thin-films with and without RMF manipulation

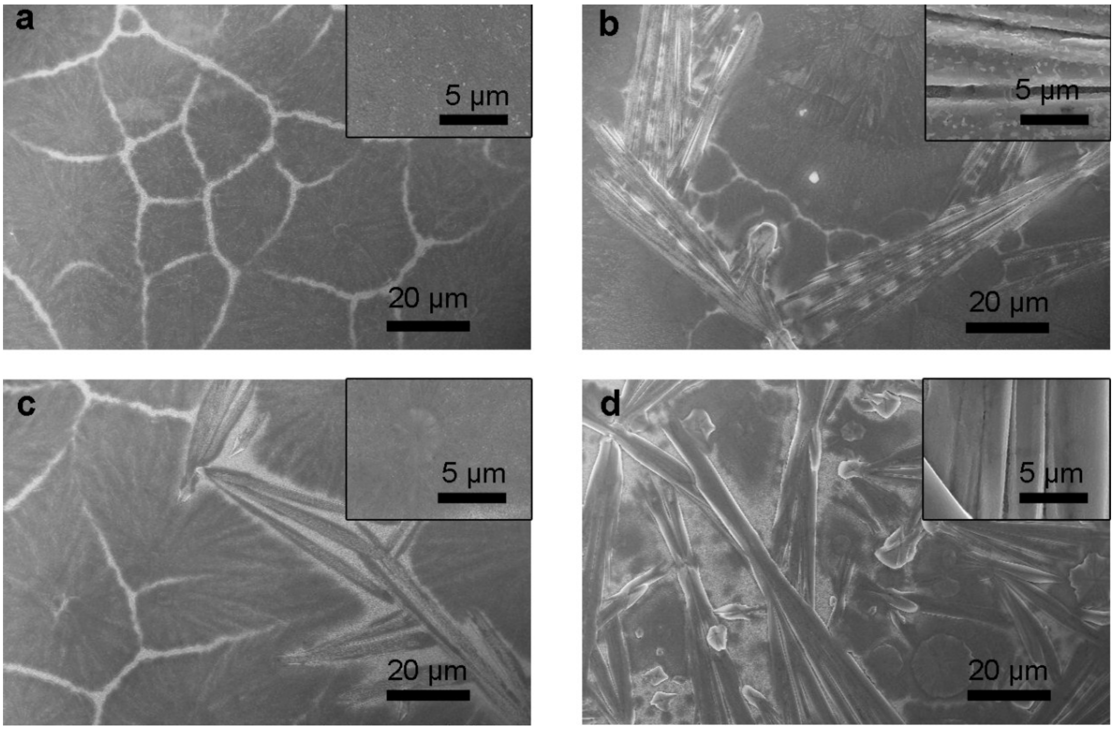

Fig. S3. SEM images of the perovskite films fabricated under the substrates' heating temperature of 120°C (a) with and (b) without RMF manipulation, and 100°C (c) with and (d) without RMF manipulation.

S4. SEM images of DMSO based perovskite thin films

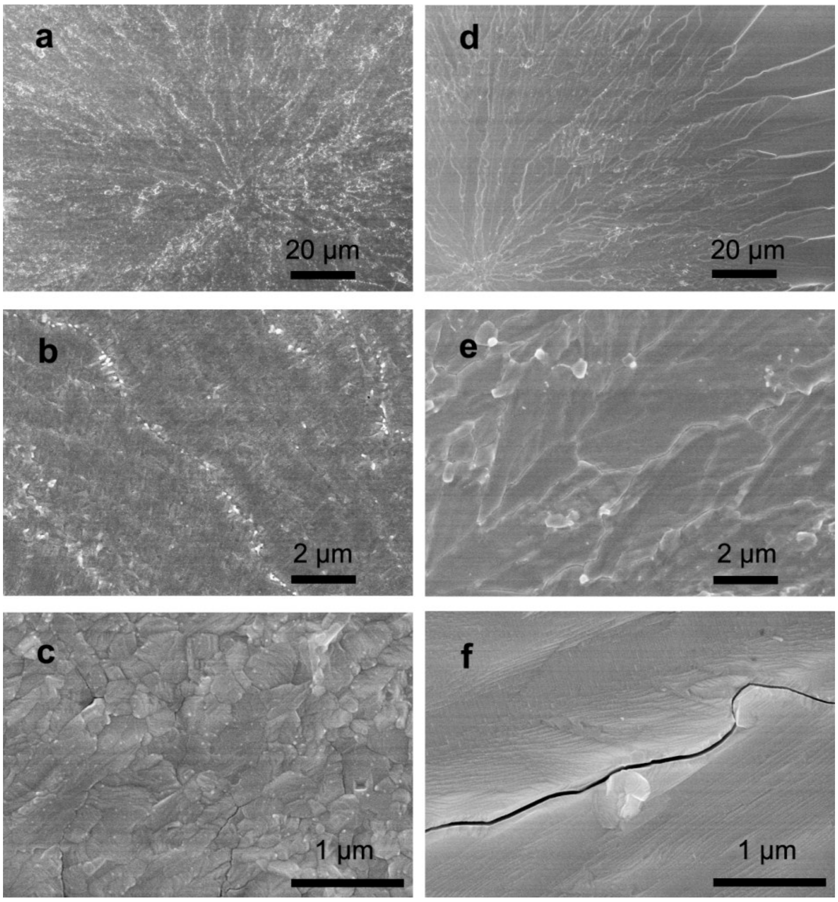

Fig. S4. SEM images of DMSO based perovskite thin-films fabricated by blade coating with (a)-(c) and without (d)-(f) RMF manipulation in different magnifications. Crack in (f) was caused by electronic beam scanning.

S5. SEM images of NMP based perovskite thin films

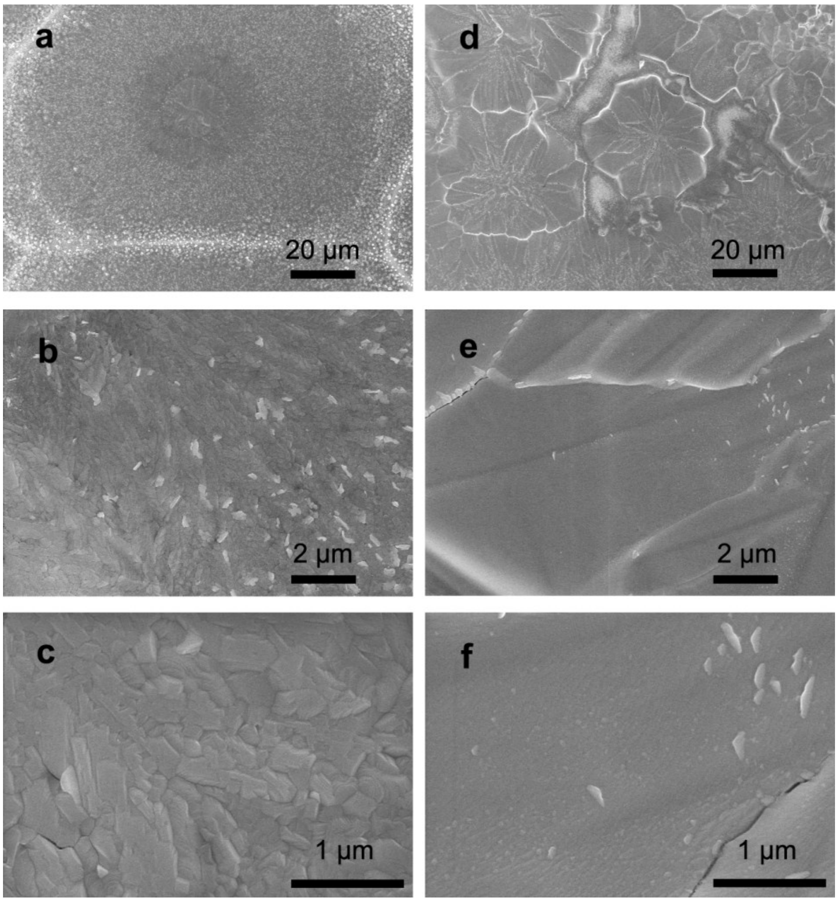

Fig. S5. SEM images of NMP based perovskite thin-film fabricated by blade coating with (a)-(c) and without (d)-(f) RMF manipulation in different magnifications.

S6. XRD patterns of RMF-induced perovskite thin-films and conventional films employing DMSO and NMP solvents

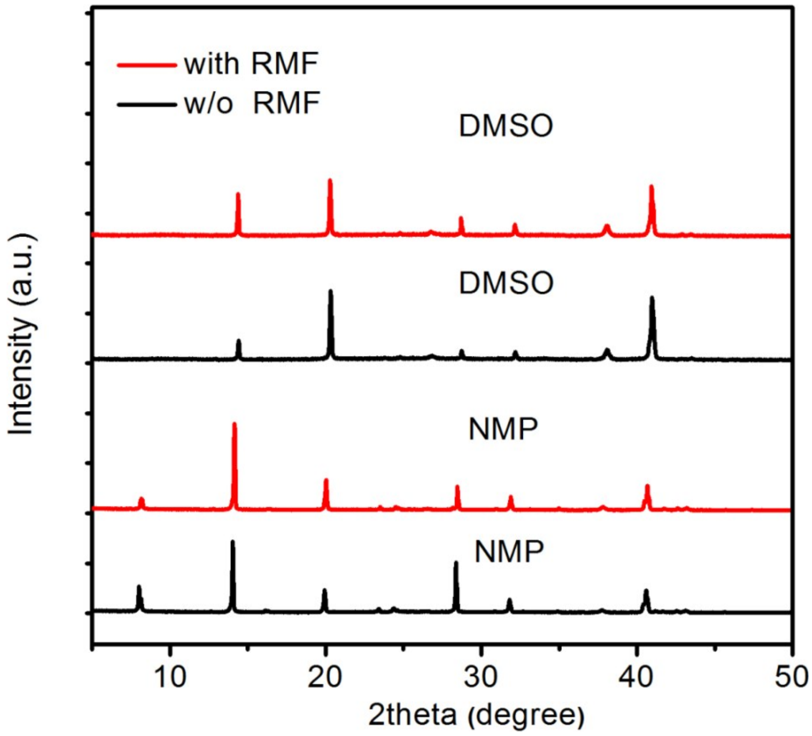

Fig. S6. XRD patterns of RMF-induced perovskite thin-films and conventional films employing DMSO and NMP solvents.

S7. IPCE spectra of the champion cells fabricated with and without RMF manipulation

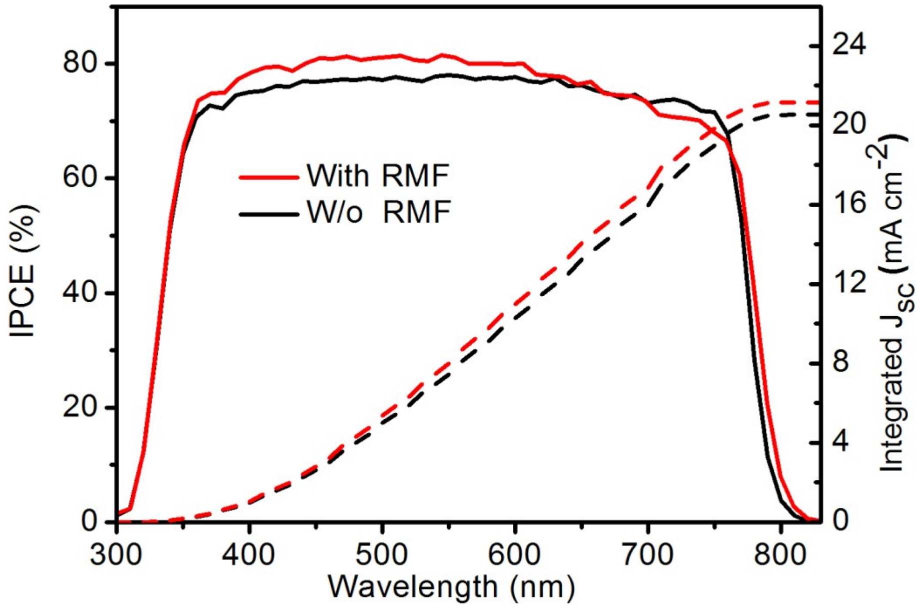

Fig. S7. Incident photon-to-electron conversion efficiency (IPCE) (solid lines) spectra and corresponding integrated photocurrent density J_{sc} (dash lines) for both two kinds of devices based on RMF-manipulated or conventional processes.

Here, the cross-over phenomenon shown in the IPCE spectra possibly should be attributed to the imbalance in molar ration of MAI:PbI_2 as reported in the previous work.[1] Generally, the stoichiometry of the precursor solution resulted in the best photovoltaic performance for the blade-coated perovskite films, and the EQE spectra also exhibited the ideal flat curve over the large range of wavelength. While for the non-stoichiometric ratio of MAI:PbI_2, the excess PbI_2 or MAI in the blade-coated film would lead to a IPCE decline in the shorter or longer wavelength region. In this work, the IPCE spectra of the conventional devices represents an approximate horizontal line due to the using stoichiometric MAI:PbI_2 molar ratios (1:1) in the blade coating, and the results matched well with the previous work.[1] However, when the RMF was introduced, the electrostatic force or Lorentz force properly would influence the movement of MA^+/Pb^+ and the final stoichiometry of the prepared perovskite films. Consequently, a slight decline at longer wavelength was observed in the EQE spectra for the RMF manipulated sample.

S8. Summarized EIS parameters for the perovskite solar cells

Table S1. Parameters employed for the fitting of the electrochemical impedance spectra (EIS) of the devices with and without RMF.

	Rs ($\Omega \cdot cm^2$)	**R1 ($\Omega \cdot cm^2$)**	**R_{ct} ($\Omega \cdot cm^2$)**	**CPE1($F \cdot cm^2$)**	**CPE2($F \cdot cm^2$)**
w/o RMF	16.75	7914	8568	1.2901E-8	8.226E-8
with RMF	19.69	5562	3930	2.2784E-8	2.321E-7

S9. The box plots of key parameter of PSCs

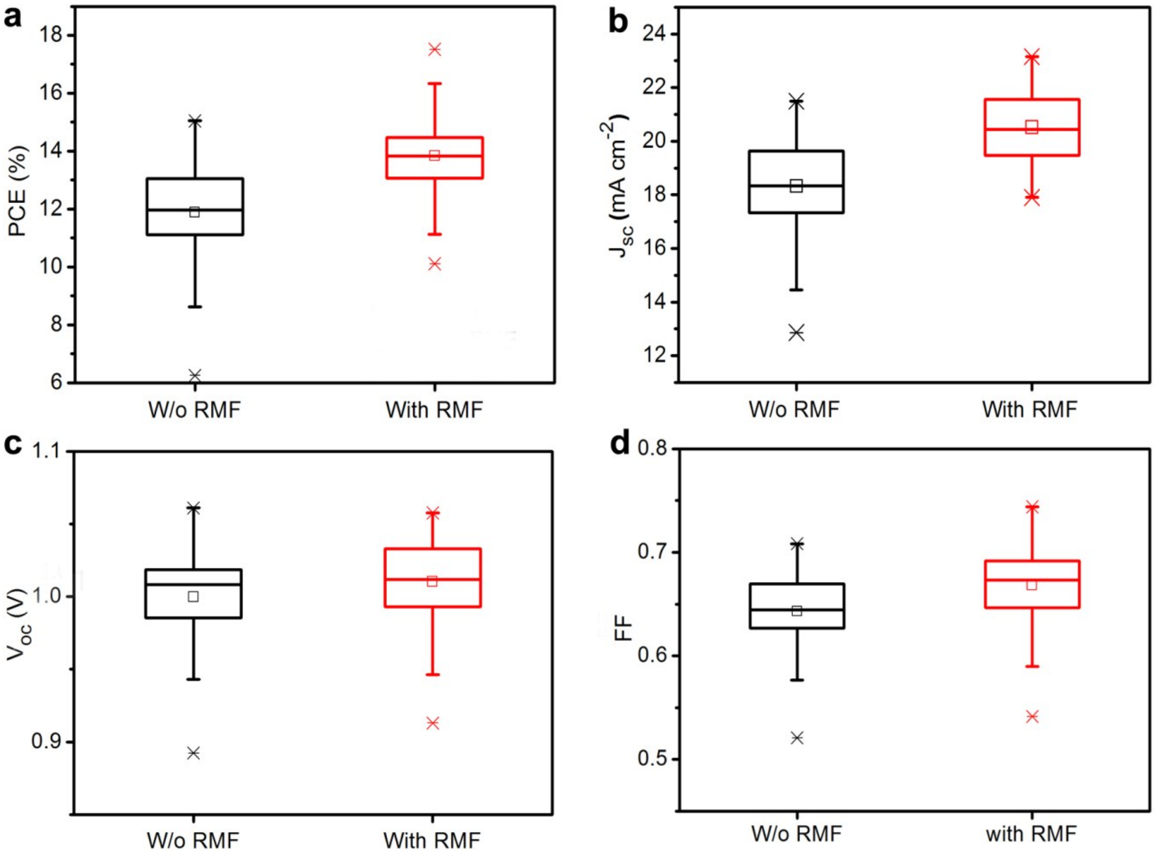

Fig. S8. The box plots of PCE, J_{sc}, V_{oc}, and FF for 50 PSC devices with and without RMF manipulations during growth of perovskite films.

S10. Hysteresis evaluation of the PSCs

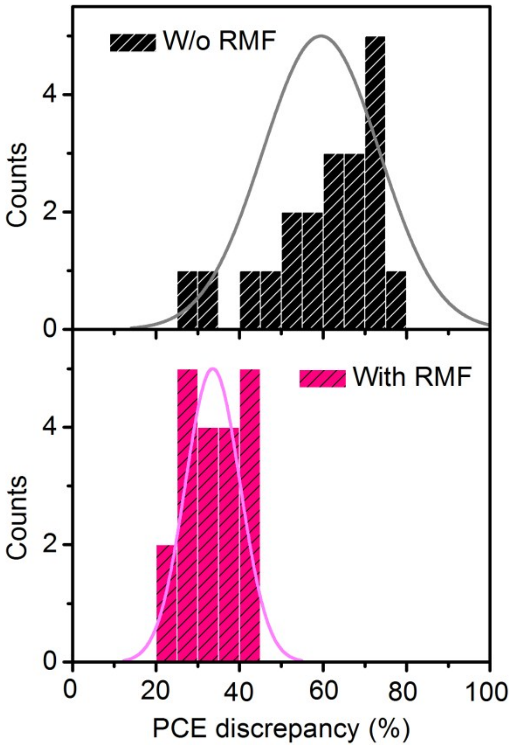

Fig. S9. PCE discrepancy of hysteresis histograms for 40 devices fabricated with and without RMF manipulation.

The *J*-*V* hysteresis was evaluated by the PCE discrepancy, which was defined as:

$$\text{PCE discrepancy} = \frac{\eta_R - \eta_F}{\eta_R} \times 100\%$$

where η_F is forward-scan obtained efficiency and η_R is reverse-scan obtained efficiency. Obviously it can be seen that the statistical histogram distribution of RMF-induced devices shows a much lower PCE discrepancy in the Fig. S9.

S11. Hysteresis evaluated by the forward and reverse scans

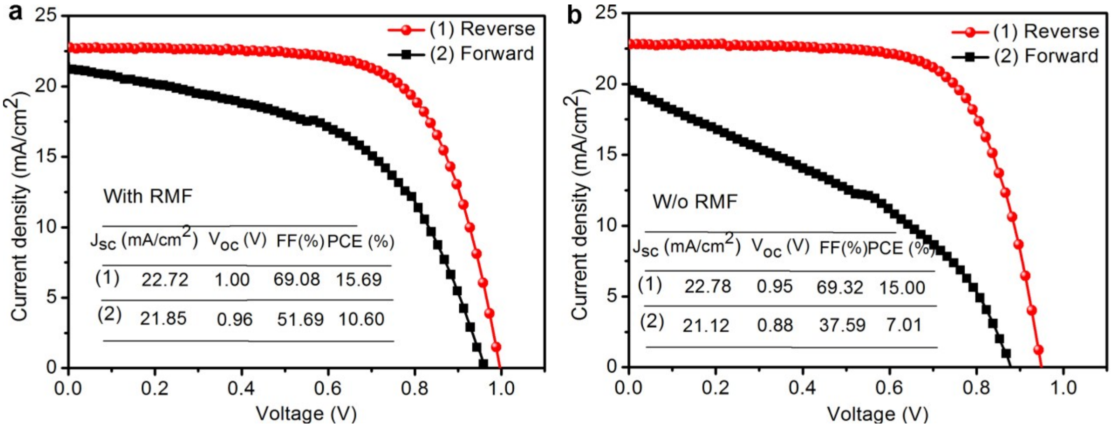

Fig. S10. Scan direction-dependent $J-V$ curves of the champion PSC devices of (a) with and (b) without RMF manipulation.

S12. Environmental stability test of unsealed PSCs

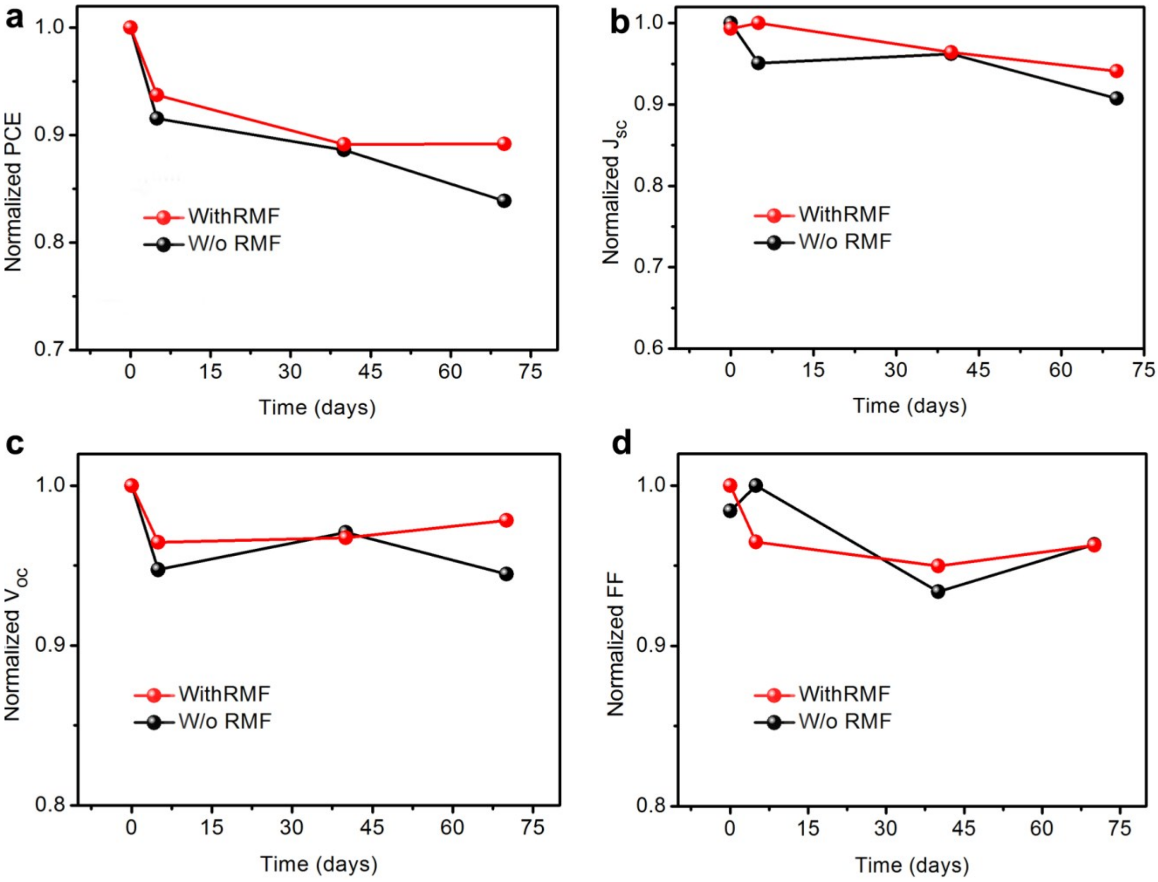

Fig. S11. Time dependence of PCE, open circuit voltage, short circuit current, and fill factor of the champion PSCs with and without RMF manipulation during growth of perovskite films for 0, 40, and 70 days stored in air at ≈25°C within 20%~60% humidity.

References:

S1. Y. H Deng, E. Peng, Y. C. Shao , Z. G. Xiao , Q. F. Dong, J. S. Huang*, Energy Environ. Sci.,* **2015**, 8, 154.